MICROMACHINED STIMULATING ELECTRODES

Quarterly Report #6

January --- March 1994

Submitted to the

Neural Prosthesis Program
National Institute of Neurological Disorders and Stroke
National Institutes of Health

by the

Solid-State Electronics Laboratory
Bioelectrical Sciences Laboratory
Department of Electrical Engineering and Computer Science
University of Michigan
Ann Arbor, Michigan
48109-2122

April 1994

MICROMACHINED STIMULATING ELECTRODES

Summary

During the past quarter, additional "EMORY" and "HMRI" wafers have been completed successfully and have been characterized. The sites have exhibited normal impedance properties without the interfacial barriers observed on some previous wafers. These wafers include both recording and stimulating designs and have gold pads with either gold or iridium sites. Experiments on penetrating the pia arachnoid and dura mater with probes having a variety of tip shapes have begun with experiments in one guinea pig. Both shallow-boron-diffused and deep-boron-diffused probe tips penetrate the pia arachnoid quite readily; the forces associated with the former are too low to be measured with our current strain gauges. No deformation of the cortical surface is seen. Neither of these probes were able to penetrate the dura, however, at least in the animal preparation used thus far. Additional experiments will be conducted during the coming quarter to obtain additional quantitative data on penetration and tissue damage as a function of probe shape.

Chronic experiments have continued during the past term to evaluate the access voltage (back-voltage) associated with bipolar stimulation as a function of site size. The access voltages across a bipolar pair generally show only slight increases over five days of stimulation (4 hrs per day) and are about 8.5V for a 50µA pulse at 100µsec/phase for a 1200µm² site and about 8V for a 1600µm² site. Histology results from the occipital lobe of one adult guinea pig stimulated at 50µA show significant tissue reaction, with a decreased number of neurons between tracts along with many reactive cells. This reaction was confined to the stimulated regions of tissue, with no cell loss or reactive cells and minimal glial reaction around the tracts remote from the active sites. Additional chronic studies are underway to confirm these findings.

Additional active probes have been fabricated using 1µm-thick LTO films covered by 0.5µm of PECVD silicon nitride over the circuit areas. All probes are fully functional with no significant incidence of pinholes during final silicon etches of as long as 3.5hrs. Small threshold shifts of approximately -0.2V have been noted during the post-metal processing, possibly due to annealing of the contacts during the dielectric depositions. The first acute experiments with these active probes will take place during the coming term. A new fabrication run of active probes has also been started to correct the etching problems noted in earlier reports. These probes should be completed by the end of the coming quarter.

MICROMACHINED STIMULATING ELECTRODES

1. Introduction

The goal of this research is the development of active multichannel arrays of stimulating electrodes suitable for studies of neural information processing at the cellular level and for a variety of closed-loop neural prostheses. The probes should be able to enter neural tissue with minimal disturbance to the neural networks there and deliver highly-controlled (spatially and temporally) charge waveforms to the tissue on a chronic basis. The probes consist of several thin-film conductors supported on a micromachined silicon substrate and insulated from it and from the surrounding electrolyte by silicon dioxide and silicon nitride dielectric films. The stimulating sites are activated iridium, defined photolithographically using a lift-off process. Passive probes having a variety of site sizes and shank configurations have been fabricated successfully and distributed to a number of research organizations nationally for evaluation in many different research preparations. For chronic use, the biggest problem associated with these passive probes concerns their leads, which must interface the probe to the outside world. Even using silicon-substrate ribbon cables, the number of allowable interconnects is necessarily limited, and yet a great many stimulating sites are ultimately desirable in order to achieve high spatial localization of the stimulus currents.

The integration of signal processing electronics on the rear of the probe substrate (creating an "active" probe) allows the use of serial digital input data which can be demultiplexed onto the probe to provide access to a large number of stimulating sites. Our goal in this area of the program has been to develop a family of active probes capable of chronic implantation in tissue. For such probes, the digital input data must be translated on the probe into per-channel current amplitudes which are then applied to the tissue through the sites. Such probes require five external leads, virtually independent of the number of sites used. As discussed in our previous reports, we are now developing a series of three active probes containing CMOS signal processing electronics. Two of these probes are slightly redesigned versions of an earlier first-generation set of designs and are designated as STIM-1A and STIM-1B. The third probe, STIM-2, is a second-generation version of our high-end first-generation design, STIM-1. All three probes provide 8-bit resolution in setting the per-channel current amplitudes. STIM-1A and -1B offer a biphasic range using ±5V supplies from 0μA to ±254μA with a resolution of 2μA, while STIM-2 has a range from 0 to ±127μA with a resolution of 1μA. STIM-2 offers the ability to select 8 of 64 electrode sites and to drive these sites independently and in parallel, while -1A allows only 2 of 16 sites to be active at a time (bipolar operation). STIM-1B is a monopolar probe, which allows the user to guide an externally-provided current to any one of 16 sites as selected by the digital input address. The high-end STIM-2 contains provisions for numerous saftey checks and for features such as remote impedance testing in addition to its normal operating modes. It also offers the option of being able to record from any one of the selected sites in addition to stimulation.

During the past quarter, research on this contract has focused in four areas. Probes continue to be fabricated for external users and distributed to them for use in their research programs. The most recent wafers processed have exhibited normal sites, both using iridium (for stimulation) and using gold (for recording). We have begun studies with a set

of penetration probes to quantify the importance of tip shape on the ability to easily penetrate the pia and dura membranes over the brain and have continued studies aimed at exploring the tissue damage and electrode impedance characteristics associated with chronic stimulation. Also during the past quarter we fabricated additional wafers of active probes using thicker layers of low-temperature deposited dielectrics (LTO and PECVD silicon nitride) over the circuit areas. The results in each of these areas are described below.

2. *Passive Stimulating Electrode Development*

The last stimulation quarterly report discussed process runs of the EMORY and HMRI mask sets. In the companion recording report, HMRI probes were reported to have good iridium adhesion and ac impedance magnitudes in the normal range. More thorough testing of a larger sample of probes, however, revealed that many of these HMRI probes had contacts that were less than ideal. Although some of the sites had ac impedances in the normal range, many initially exhibited impedances indicative of an open site. It is believed that this problem was caused by an interfacial oxide between the polysilicon and the titanium. We were able to break down the oxide on these high-impedance sites by applying a dc bias (as low as 0.1V for many sites and as high as 20V for others) between the pad and the site. Once broken down, the sites maintain their low impedances. Probes from this wafer were sent only to those investigators using them for stimulation (Dr. William Agnew of Huntington Medical Research Institutes and Dr. Andrew Hoffer of Simon Fraser University) since, through the process of activation, the sites should break down. We are awaiting reports from these investigators on their experiences with probes from this run.

During the present quarter, new runs of EMORY and HMRI wafers were completed. All probes have gold bonding pads and iridium recording sites. A large sample of probes from both masks have been tested and show consistent normal ac impedances at 1kHz. Examples of impedances obtained from a variety of these probes are shown in Table 1. Figure 1a shows the tip of a probe from this process run. Within the next few weeks, probes from these process runs will be prepared and provided to their respective investigators.

PROBE TYPE	APPROX. SITE AREA	IMPEDANCE RANGE *(n=number of sites tested)*
3-SHANK-1	48µm²	4.0-5.6MΩ (n=24)
DEPTH 1	64µm²	2.3-3.7MΩ (n=15)
NANO 8	75µm²	3.1-5.8MΩ (n=16)
3-SHANK-2	108µm²	2.5-3.5MΩ (n=24)
EMORY	408µm²	900kΩ-1.4MΩ (n=16)
SCHMIDT	494µm²	900kΩ-1.1MΩ (n=12)
SCALAR INVADER	1018µm²	500-700kΩ (n=16)

Table 1: Results of ac impedance tests on new EMORY and HMRI probes. The tests were performed by passing a 1kHz, 20mV sinewave through a reference in saline using an HP 4194A Gain/Phase Analyzer.

Also during the last quarter, another wafer containing the chronic stimulation probes used in the *in vivo* current flow and impedance studies was etched out. Processing on this and several other wafers is complete up to the final etch step allowing us to complete probes on an as-needed basis. A scanning electron micrograph of one of these probes is shown in Fig. 1b.
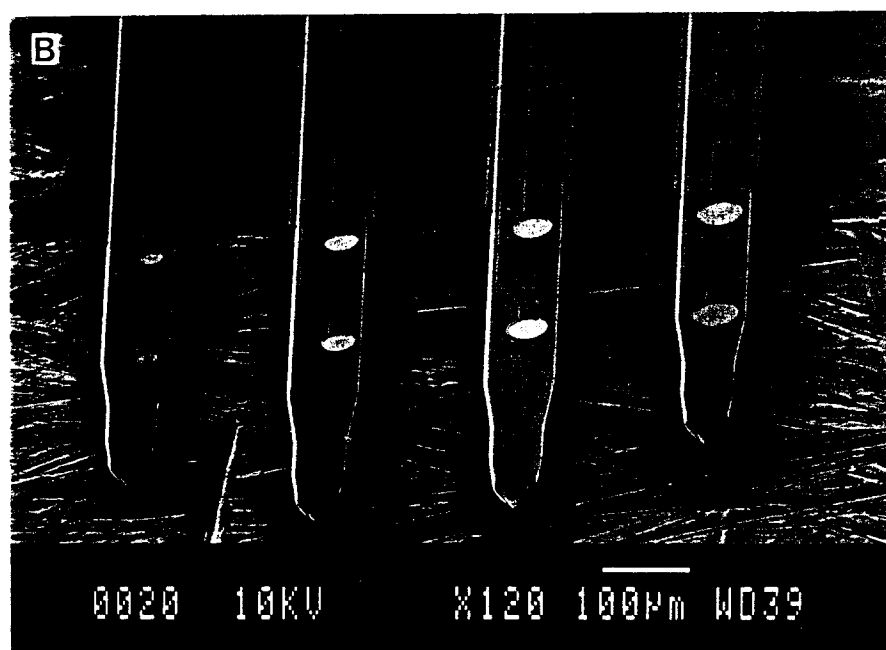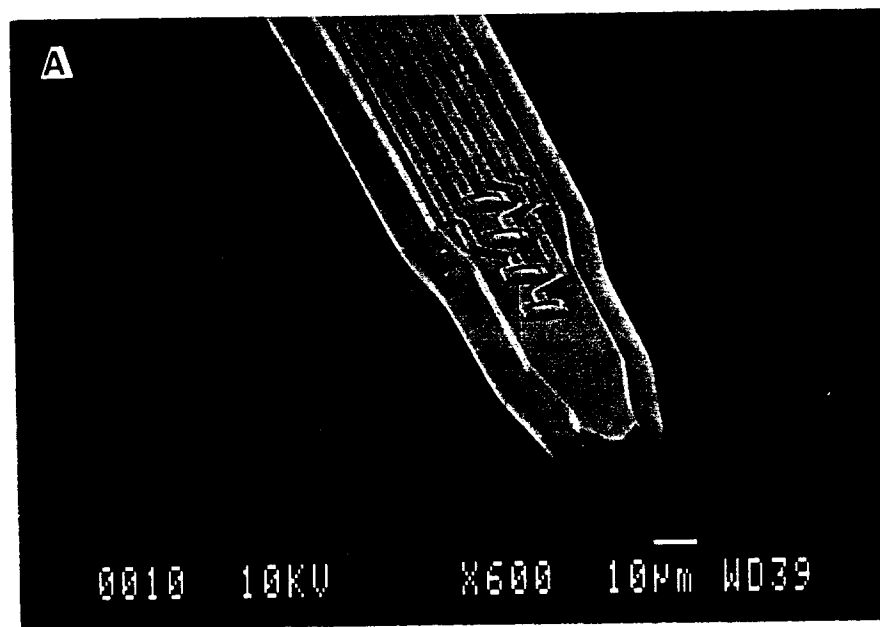
Fig. 1: Scanning electron micrographs of probes from recent process runs. A very narrow, deep diffused recording probe tip is shown in 1a. Sites on this shank are spaced at 25μm. In 1b, a stimulating probe to be used in the chronic current flow and impedance studies is shown (see Section 2.2). Shanks on this probe are spaced at 200μm and sites range in size from 400-1600μm².

3

2.1 Penetration Studies

In previous reports we have discussed the penetration study and its various aspects in more detail. Briefly, a set of probes, referred to as PNTPROBES, have been designed and fabricated incorporating different tip and shank geometries in order to study the tissue coupling, insertion forces, and tissue damage associated with inserting the probes through the pia arachnoid and dura mater of guinea pigs and other experimental animals. We expect that theses probes will help to define the optimum probe shank geometry: one that will provide the best combination of low penetration force with minimal cortical surface dimpling, minimal tissue damage and/or reaction along the insertion track, and maximum tissue-electrode coupling.

During the past quarter, we have begun performing cortical penetrations to evaluate the forces required for penetration. The penetrations and data collection are controlled with a Macintosh IIx computer. The entire data acquisition system is shown in block diagram form in Fig. 2. The system is automated using LabVIEW, a graphical programming language for instrumentation (the front panel of the *virtual instrument,* used to control and monitor the system, is shown in Fig. 3). For the penetration force study, the system uses a voltage-driven constant current source to force a known current through the strain gauge, and then the voltage drop across the strain gauge is sensed and amplified by a differential amplifier before being digitized by a National Instruments data acquisition board (daq). Each voltage sample is linked to a microdrive position sample which is acquired at the same time so that later we can calculate the strain gauge resistance, the stress in the probe shank, and finally the penetration force at the tip of the probe. The strain gauge resistance is calculated from the digitized voltage, the current source transconductance, and the amplifier gain. Due to a system constraint (LabVIEW requires a DMA controller for analog output) we have been unable as yet to use the analog output of the daq to control the current output, but have instead simply used an externally generated reference voltage and measured that with a daq input for resistance computations. This limitation can easily be overcome by either installing a DMA controller or possibly with software that does not require the DMA. We can then use this same system for measuring the tissue impedance.
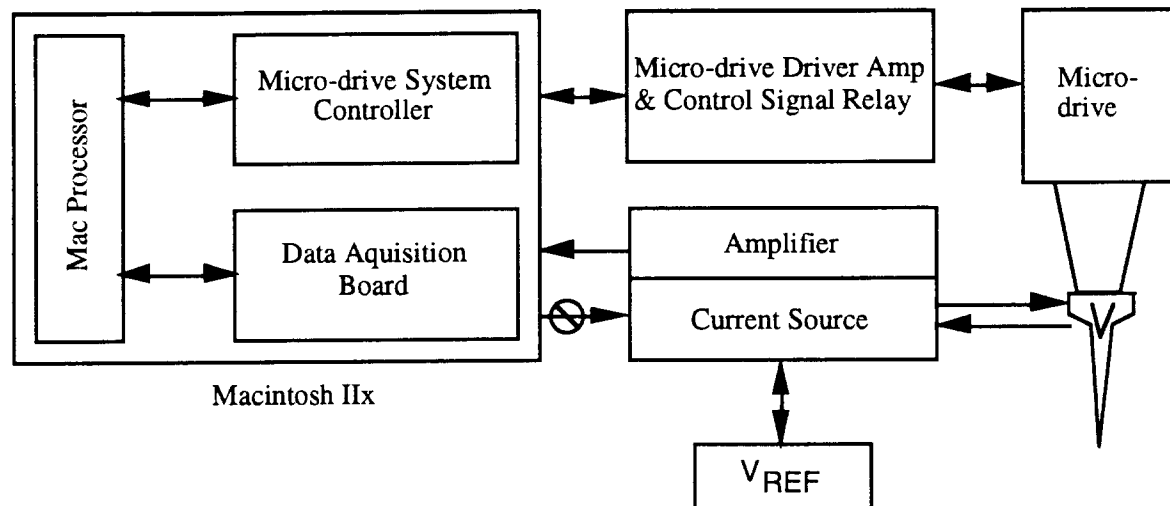

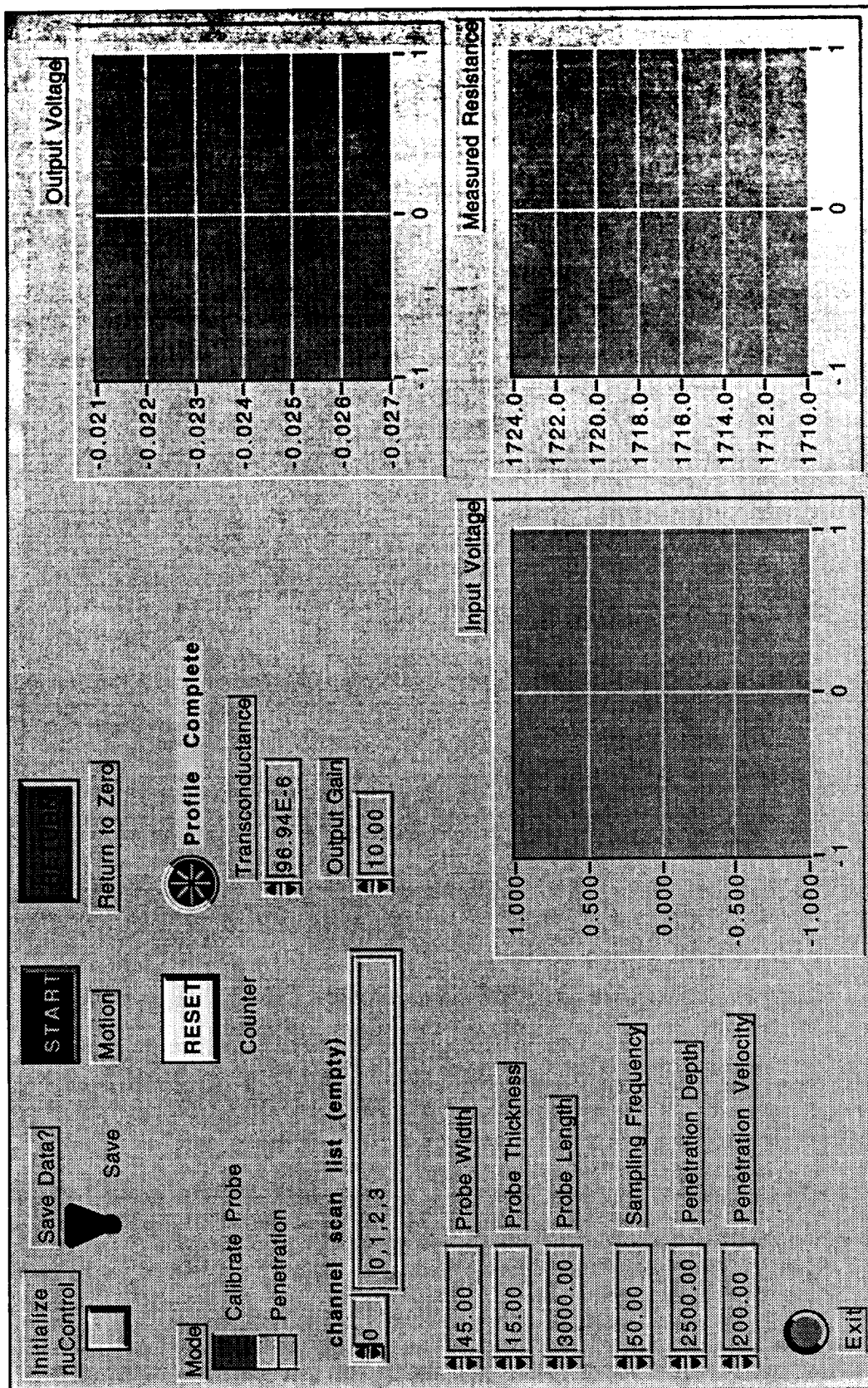Fig. 2: The block diagram of the data acquisition system.

Fig. 3: Front panel display for controlling and monitoring the data acquisition and microdrive controller.
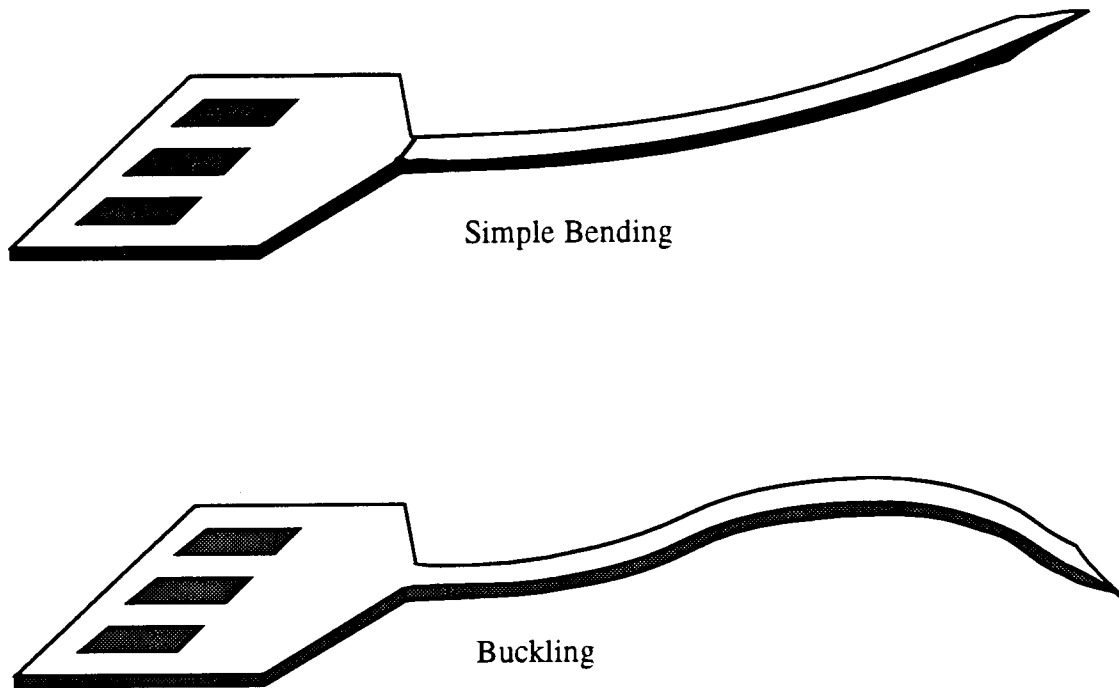
Simple Bending

Buckling

Fig. 4: The two common modes of deflection for a microprobe shank pressed against the pia arachnoid.

Thus far we have been unable to get a true characterization of the relationship between the axial force at the tip of a buckled probe shank and the resistance (and therefore strain) measured by the strain gauge. There are two ways in which the resistance vs. strain can be characterized as shown in Fig. 4: 1) by a simple bending of the probe shank with a known deflection and, 2) by buckling of the probe shank with a known axial tip deflection. The simple bending is easy to characterize since it has a well-known and quite simple solution. The solution to a buckling shank is not well known. Figure 5 shows that the same amount of tip deflection for the two different cases results in very different changes in the resistance of the strain gauge. It turns out that once a beam buckles, the solution is nonlinear and requires use of elastic theory; a closed form solution is not easily found. Thanks to Prof. Noel Perkins (of the Mechanical Engineering and Applied Mechanics Department) and his student Chung-Long Lu, a numerical solution is being computed that will give us this relation. We can then use the resistance data that has already been acquired along with the microdrive position to characterize the probes and then calculate the probe shank strain and penetration forces.

In the previous quarterly report, it was mentioned that we hoped to be able to characterize each probe individually prior to actual use in the study. It was found that this will not be possible in the case of the very sharp shallow boron diffused tips since the shallow boron point tends to break off when pushed against a hard object with enough force to sufficiently buckle the shank for characterization of the strain gauge. This is not expected to be a problem since the percentage change in resistance of the strain gauge for a given deflection should be fairly constant across all of the probes though the base or undeflected resistance may vary somewhat. The undeflected resistance can easily be measured for each probe.

We have performed initial penetrations and recorded the strain gauge resistances using the extreme cases of the probe tip geometries in order to get a feel for how much

variability there is. We attempted to penetrate the dura mater of a mature 700gm guinea pig with a 10° 65μm-wide shallow-boron-diffused tip, the PSA1065-SB. Repeated attempts only resulted in breaking the probe shank. Previous studies have indicated the feasibility of penetrating the dura mater with probes that had tips that were considerably less sharp. The probes in those studies were also about twice as thick as the probes used for this study, which affects the stiffness of the shank by the square of the thickness. Another possible factor was the advanced age of this particular guinea pig, which likely resulted in a tougher dural membrane. We will attempt to penetrate the dura of a younger guinea pig simply for evaluation purposes; for normal implants, the probes are not required to penetrate the dura mater but only the pia arachnoid under it.
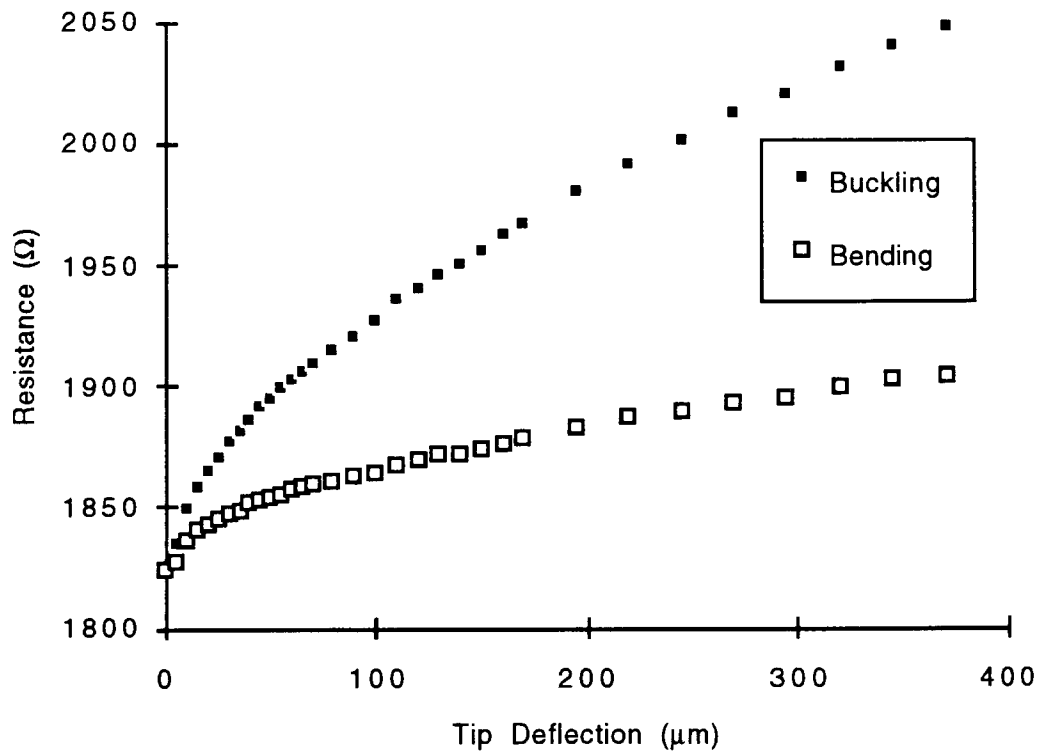
Fig. 5: Strain gauge characteristic response curves versus tip deflection in the axial direction.

Figure 6 shows a typical attempt to penetrate the dura mater with the strain gauge resistance measured as a function of the microdrive position. The microdrive was advanced at a constant velocity of 200μm/sec, and the position and resistance were sampled at 50Hz. Brain pulsation, due mainly to respiration, adds an undesirable component to the measured data. A 45° deep-boron-diffusion-tipped 65μm-wide probe, the PSA4565-DB, was unable to penetrate the dura mater either, which was expected after the failure of the much sharper probe. Several penetrations of the pia arachnoid with the PSA1065-SB were performed without being able to measure any change in resistance of the strain gauge nor observe any visual indication of probe shank buckling or brain surface dimpling. While this is a desirable outcome, it makes it very hard to quantify insertion force except to say that it is lower than the measurable limit.
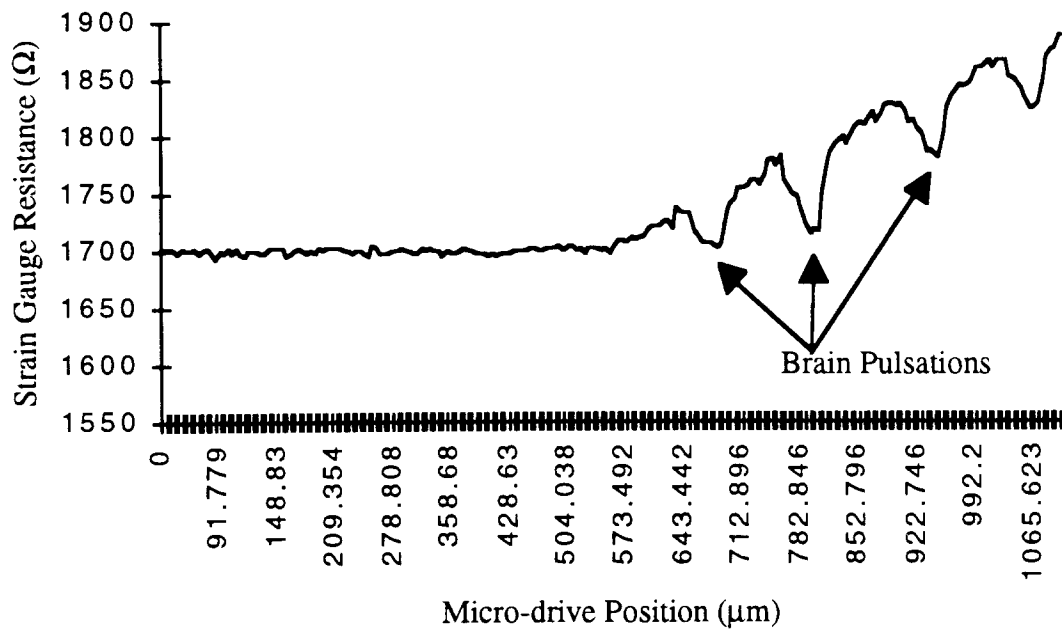
7

Fig. 6: Attempt to penetrate the dura mater with a 10° 65μm-wide shallow-boron-diffused tip.

The PSA4565-DB was also used to penetrate the pia arachnoid, which it did very easily. It also penetrated so easily that it was very difficult to see the change in the strain gauge resistance due to the fact that it was on the same order as the system noise level as can be seen in Fig. 7. Using a 7-point moving average on the data helped to clean up the noise as shown in Fig. 8. Even so, brain pulsation still had a substantial effect on the data because it is so large. Figures 9 and 10 show another penetration that was performed nearer the edge of the area of the animal's head with the dura mater reflected to expose the pia. This demonstrates an important aspect of penetration: proper alignment of the probe shank to the direction of travel and a normal/perpendicular approach to the brain surface (Fig. 11). The curved surface of the brain can easily cause the approach of the probe to be other than normal. This, in turn, causes the probe tip to shift slightly off axis as it starts to press against the surface of the pia. As the probe continues to penetrate, the entire shank is deflected more and more, causing a change in baseline resistance. This will tend to cause more damage to tissue on the loaded side of the probe shank. For this experiment this can be corrected by adjusting the stalk attachment to the microdrive to properly align the probe shank to the direction of travel and the adjust the microdrive to achieve a direction of travel normal to the brain surface. After each adjustment, a penetration shows whether the adjustment was good enough. Such repeated penetrations are not possible when using the recording or stimulating probes so the problem will have to be addressed further.

Inspection of the probes after the penetrations were performed revealed that the tips were still intact. The blunt tip was expected to be satisfactory, but there was some question about the ability of the sharp probe to withstand penetration. There were no problems in this regard.
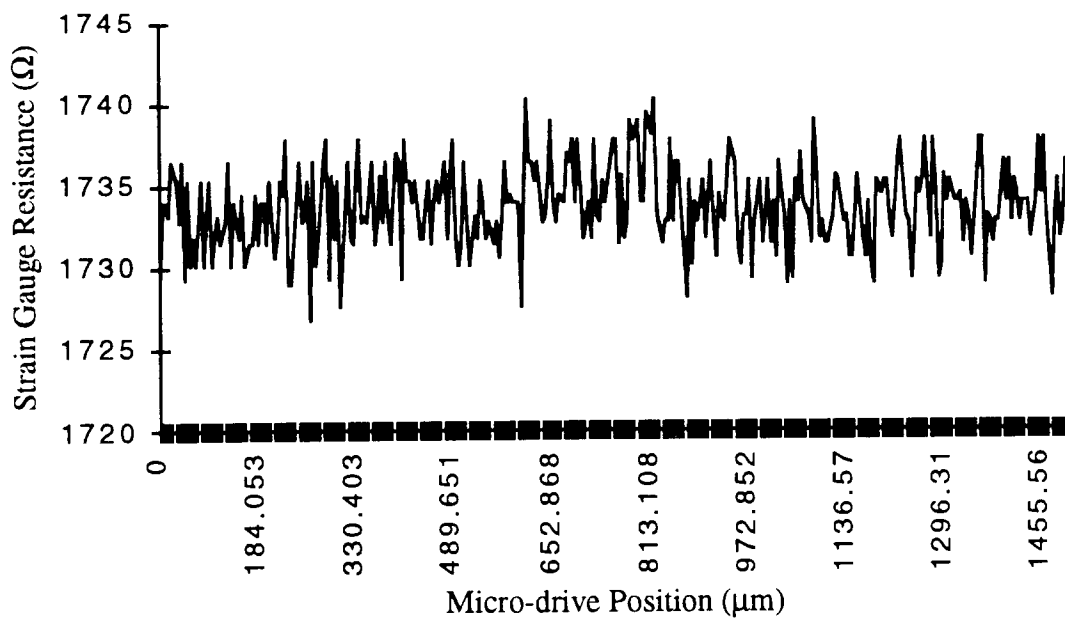
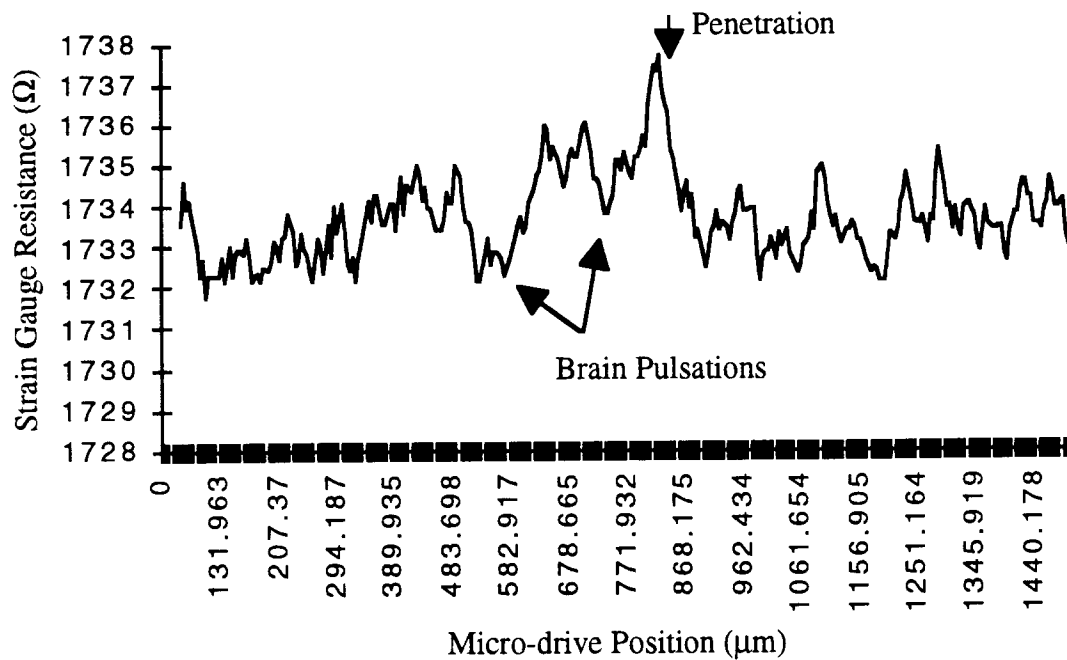Fig. 7: Pia arachnoid penetration with a 45°, 65µm-wide deep-boron-diffused tip.

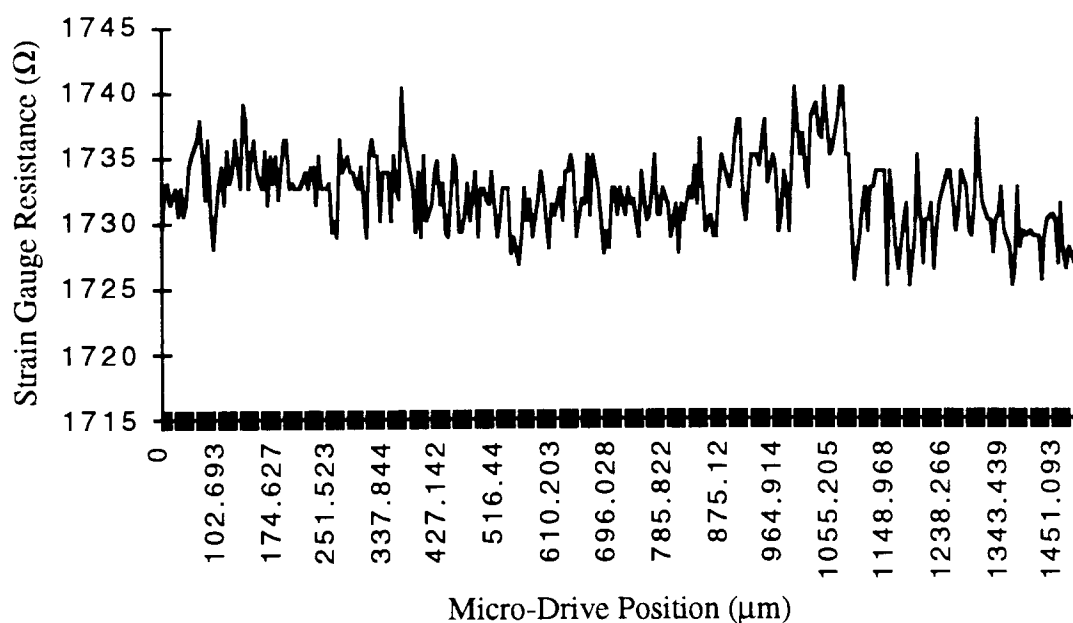Fig. 8: The same data as in Fig. 7 after smoothing with a 7-point moving average.

9

Fig. 9: Pia arachnoid penetration with a 45° 65μm-wide deep-boron-diffused tip that demonstrates the effect of a misaligned penetration.
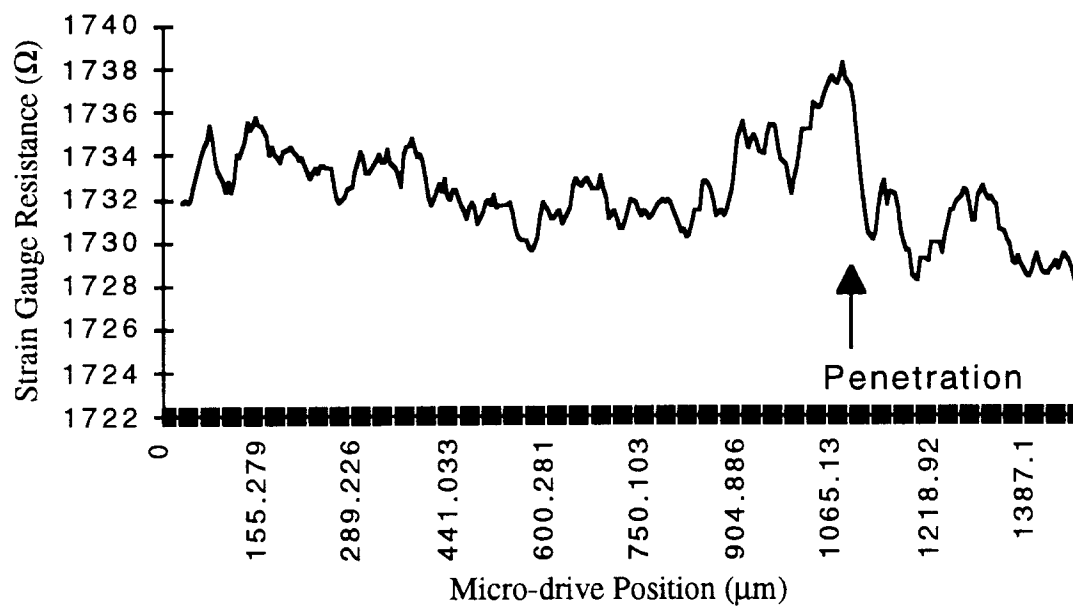

Fig. 10: The same data as in Fig. 9 after smoothing with a 7 point moving average.
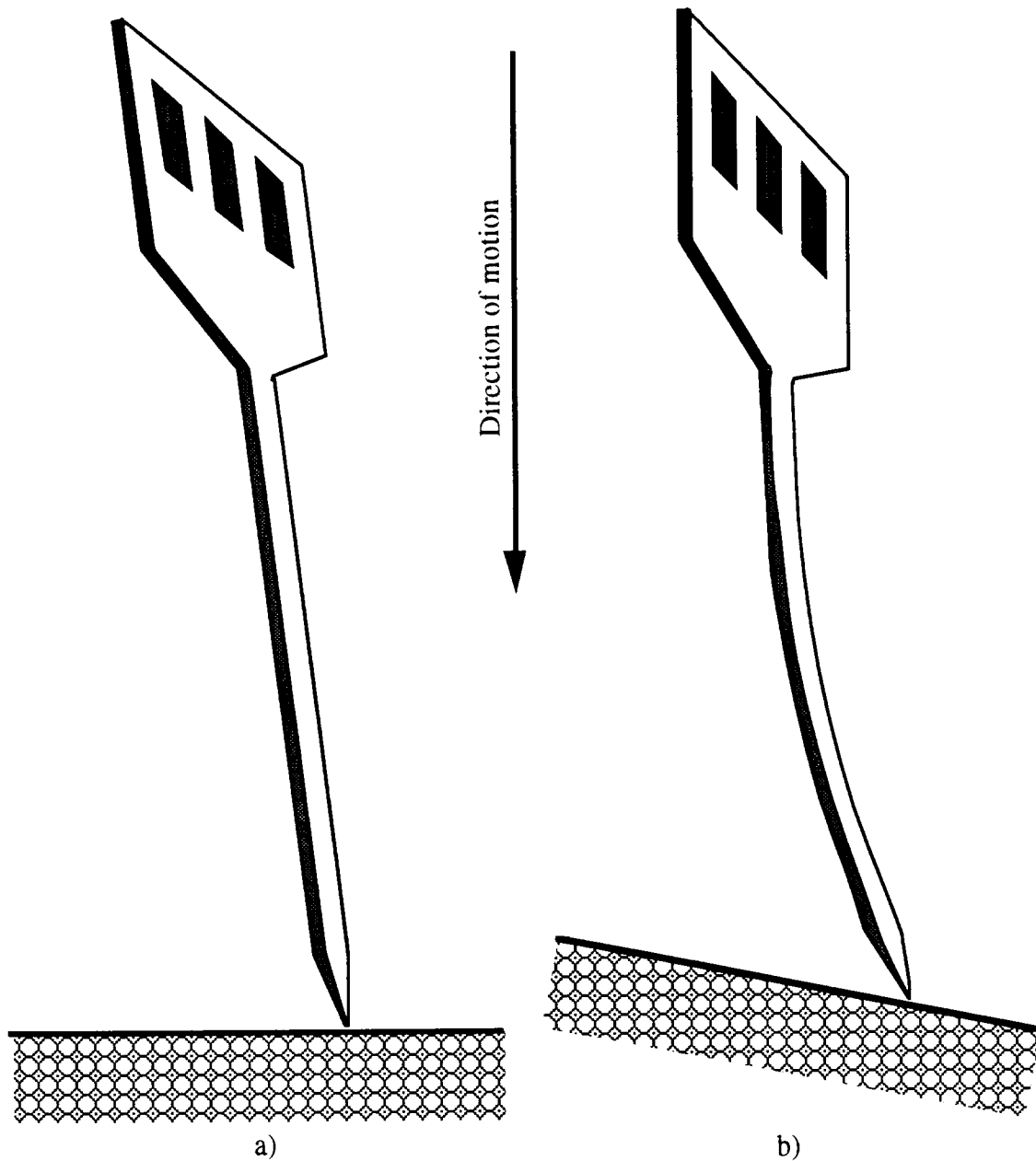
10

Direction of motion

a)

b)

Fig. 11: The two types of probe misalignment, a) misalignment of the probe with the direction of travel, and b) misalignment of the direction of travel with the normal to the surface of the brain.

Our results thus far indicate that in future penetrations we should reduce brain pulsations as much as possible. We will also look into ways to reduce the amount of noise in the measurement system. Use of younger animals for dura mater penetration will also be explored in the coming quarter along with increasing the sensitivity of the strain gauges. We will also translate the resistance changes into force and compare against the measurements from our earlier work. Chronic implants of the artificial neuron probe and the tissue resistivity probe are expected to start in the next few weeks along with continued evaluation of the acute penetrations.

11

2.2 In-Vivo Current Flow and Impedance Studies

This past quarter work has continued with passive stimulating probes. A chronic implant experiment was accomplished featuring a probe with varying site sizes. Also, the first histology results from a previous chronic stimulation experiment have been received and analyzed.

A chronic stimulation experiment was performed using a passive four-shank probe with a silicon cable. Each shank had a pair of iridium sites. The sites of each pair were the same size, but the size varied between pairs. The sizes were 400, 800, 1200, and 1600μm^2. The iridium sites were activated to a charge density of approximately 100mC/cm^2. The probe was implanted in the right occipital cortex of an adult guinea pig following the surgical procedure described in previous reports. The animal was allowed to recover for a period of 10 days, prior to the start of stimulation.

The stimulation protocol was as follows. Bipolar stimulation was performed between the sites of the two largest site pairs. The level of stimulation was 50μA. The stimulation waveform was a positive-first biphasic pulse, 100μsec per phase, followed 1msec later by a negative-first biphasic pulse. This waveform was presented for four hours between each site pair. Impedance and access voltage data were taken before, during (at 30 minute intervals), and after the stimulation period. This procedure was repeated for five straight days. A typical plot for access voltage is shown below. This waveform was an average of 200 records sampled at 100kHz.
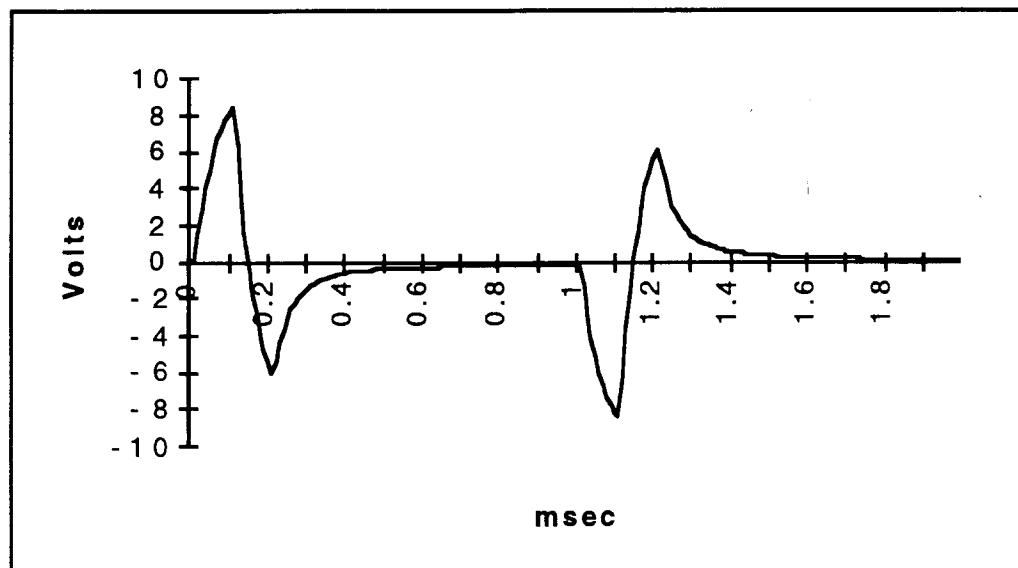

Fig. 12: Typical access voltage plot as measured across the bipolar electrode pair.

Due to the short length of the current pulse, the "capacitor" formed by the electrode-tissue interface never fully charges. This explains the exponential shape of the pulses. The following pulse is lower than the lead pulse because the it takes time for the charge built up in the oxide to dissipate (the capacitor is discharging). The charge remaining from the lead pulse will decrease the voltage reached by following pulse. Stored charge dissipation also explains the long tail in the following pulse. The best information we can get for access

12

voltage is the maximum value it achieves during the lead pulse. This information is shown in Figs. 13 and 14.
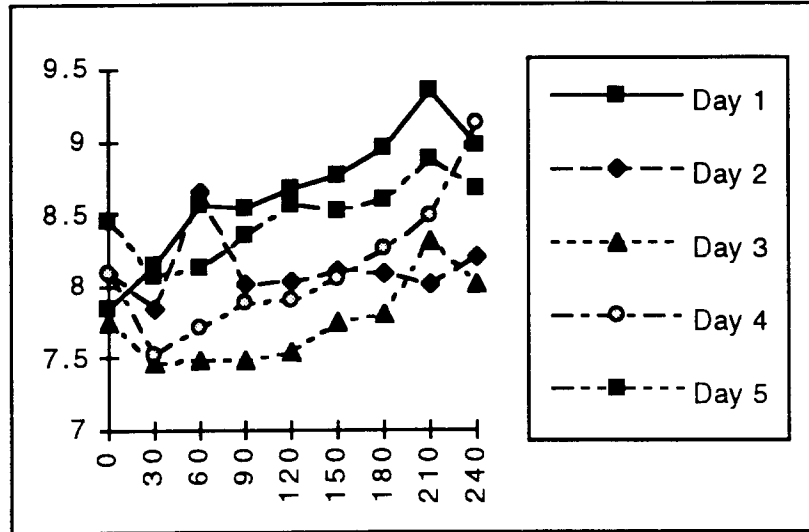

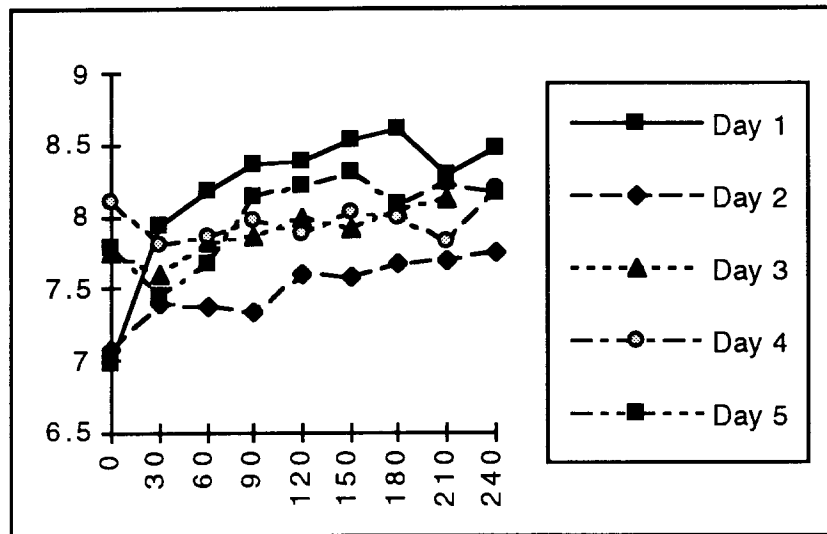Fig. 13: Access Voltage vs. Time for 5 days of Stimulation. Site Size = 1200μm^2

Fig. 14: Access Voltage vs. Time for 5 Days of Stimulation: Site Size = 1600μm^2

The above plots show the maximum access voltages during five days of stimulation. The larger site sizes have a lower access voltage, as would be expected. Also, we continue to see the trend of rising voltage during stimulation, though it is not as pronounced as in previous experiments.

Histology results from the first experiment (run in December) were made available in this past quarter. The experiment will be reviewed briefly. A three-shank passive probe with a silicon cable was implanted in the occipital lobe of an adult guinea pig. On each shank was a pair of activated iridium sites. The sites were 1000μm^2. The stimulation protocol was the same as above except for the site pairs for stimulation. One pair was

chosen so that stimulation would occur along the shank and the other was chosen so that stimulation would occur between two shanks. It is theorized that encapsulation of the probe shank will cause a difference in impedance and access voltage for the two pairs. The animal was sacrificed four weeks after cessation of stimulation.

Eighty-eight tissue sections, each 6μm thick, were prepared. This set of tissue slides contains the tracts of the three-shank electrode up to the tip. With knowledge of both the probe's position in the brain and the method used to section the tissue, we were able to estimate the position of the stimulated tissue. The between-shank stimulation took place at sites 300μm from the tip of the middle shank (the middle shank is 100μm longer than the outer shanks). By counting backwards from the eighty-eighth slide (where the last trace of the middle-shank track is present) in 6mm increments, one can estimate that slides 35-40 contain the stimulated tissue. Figure 15 shows the position of the sections described below in relation to the probe.
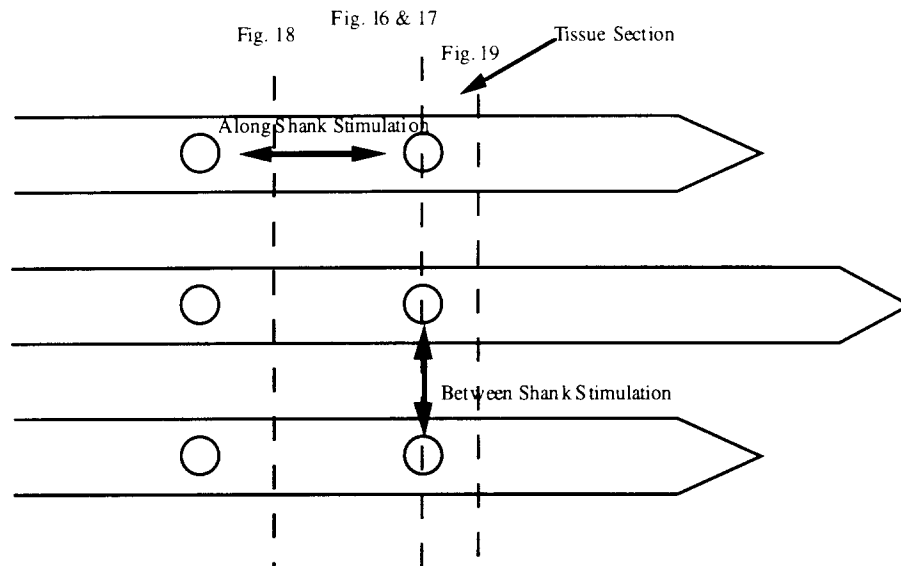

Fig. 15: Tissue sections in relation to stimulation site position.

Sections through the tracts at the level of sites where stimulation occurred showed moderate tissue reaction (Figs. 16 and 17). There was a decreased number of neurons between tracts along with many reactive cells. Reactive cells were also visible around the tracts. In most of the sections through the region of cortex above the level where stimulation occurred, only two of the three tracts were visible (Fig. 18). In these sections the neuropil appeared normal with no cell loss discernible and minimal glial reaction around the tracts. Reactive cells, however, were visible associated with the most lateral tract.

In sections through the tissue beneath the stimulation sites, three tracts were still visible. As with the sections above the stimulation sites, although there was only minimal gliosis and no discernible cell loss, many reactive cells were present (Fig. 19), even 50μm below the level where cell loss was seen. Reactive cells could still be observed, mostly associated with just one of the probe tracts. At the very bottom of the tracts only occasional reactive cells were seen and the neuropil once appeared normal with no cell loss and minimal glial reaction around the tract. This suggests that either the stimulation conditions or some other manipulation in this experiment resulted in tissue damage and subsequent tissue reaction. We will therefore repeat the stimulation and placement conditions in additional animals.

14

Fig. 16: Histological tissue section at the level of stimulation for a three-shank probe. The section was taken four weeks post-stimulation.
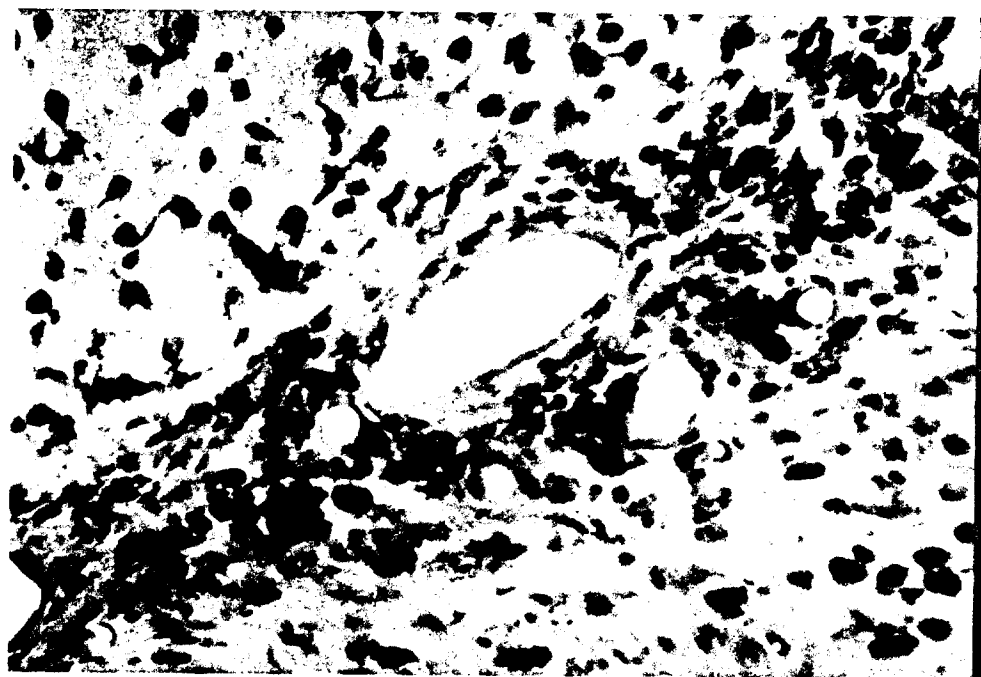

Fig. 17: A second section at the level of stimulation, similar to Fig. 16.

Fig. 18: Histological section above the area of stimulation. See Fig. 15.

Fig. 19: Histological section taken 50µm below the stimulating sites.

Unfortunately, the tissue samples that would have showed the effects of along shank stimulation are not available. It appears that the shank's position was such that only one site was in tissue (the other was in a nearby fissure) and the majority of the distance between the sites was not in tissue.

It is difficult to correlate these findings with any of the electrical measurements taken since only tissue for between shank stimulation could be examined and since the impedance and access voltage results were seen as suspicious in the first place (see the last two reports). However, this does give our first look at the long-term effects of stimulation on tissue in this current set of experiments.

In the next quarter, we will continue chronic stimulation experiments. We expect to receive histology from several animals that were completed earlier. Also, we will take a closer look at our probe activation methods and stimulation protocols in an effort to reduce the access voltages we currently see for bipolar stimulation.

3. Development of Active Stimulating Probes (STIM-2)

During the past quarter, more extensive experiments were performed in the fabrication of active stimulating probes using a thick LTO deposition (about 1µm instead of the 0.46µm reported last quarter) and a PECVD nitride deposition (about 0.5µm) over the CMOS circuitry. We tested the stimulating chips again just prior to the final micromachining step and then afterward with very encouraging results. These top dielectric layers were thick enough to protect the CMOS circuitry in the EDP etchant during probe separation. We still have a corner undercutting problem after probe separation but it will be fixed by off-axis alignment as mentioned in the last quarterly report. Another new run using this option is being processed, and we are expecting probes from this run before the end of the summer.

CIRCUIT TEST RESULTS

STIM-1B

STIM-1B is the monopolar version of the stimulating probes. In this case, site address information is entered serially using the clock to increment an on-chip counter. The counter state is decoded to select the desired site, which receives the externally-generated current via an on-chip multiplexer. Figure 20 shows the operation of the monopolar probe. The upper trace is the input clock signal, which is used to set the site address. The address here is set first at site #1 and is then switched to site #7. The middle trace shows the site-drive signal, which in this case is an arbitrary waveform used for illustration only. The bottom trace shows the measured voltage output waveform at site #1 across a 10kΩ resistor. Site #1 receives input only when addressed.

STIM-1A

STIM-1A is a medium-complexity version of the stimulating probes which is used for bipolar stimulating applications. To effectively stimulate the tissue, a bipolar current drive scheme is adopted; both current sourcing and sinking operations are performed simultaneously on the sites during the active stimulating cycle. In the bipolar case, eight

bits of serial data are used to select two sites. The subsequent 8 bits of current amplitude data is then used on-chip to generate the stimulus current for the first site using a current-output digital-to-analog converter (DAC). This current is mirrored to the second site to form a bipolar pair. Figure 21 shows the operation of the bipolar probe. The upper traces are the 16 input clock signals, which are used to control the shift register while it loads external data information. The center trace shows the site-drive data signals (address and current level). The address here is set first at site #5 to generate maximum sinking current and is then switched to provide maximum sourcing current. The bottom trace shows the measured voltage output waveform at site #5 across a 10kΩ resistor. Site #5 properly provides both maximum sourcing and sinking currents alternatively when addressed. Figure 22 shows another operation of the bipolar probe. The center trace shows the site-drive data signals. The current level here is set first at (1111111) to generate the maximum sourcing current and is then switched to provide a medium level of sinking current at (0111111). The bottom trace shows the measured voltage output waveform at site #5 across a 10kΩ resistor. Site #5 properly provides stimulating current alternatively when addressed. In Fig. 23, site #5 is selected and a full scale sourcing current (1111111) is provided while alternating different addresses: (100) to (010). The bottom trace shows the measured voltage output waveform at site #5 across a 10kΩ resistor.
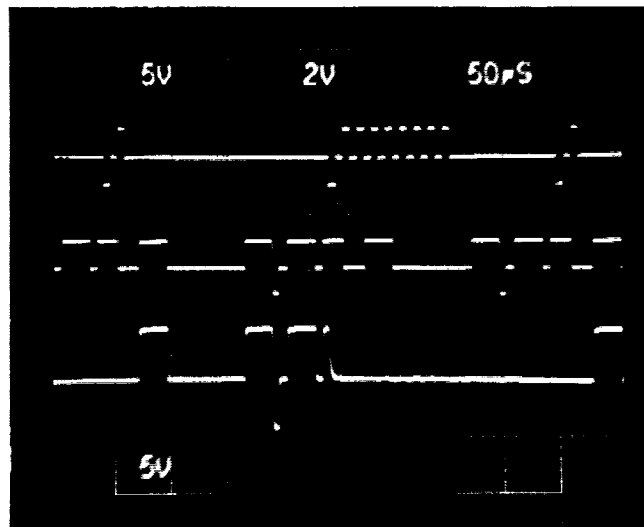

Fig. 20: Operation of the monopolar probe. Upper trace: input clock signal; middle trace: site-drive signal, which in this case is an arbitrary waveform used for illustration only; bottom trace: measured voltage output waveform across a 10kΩ resistor. Site #1 receives input only when addressed.
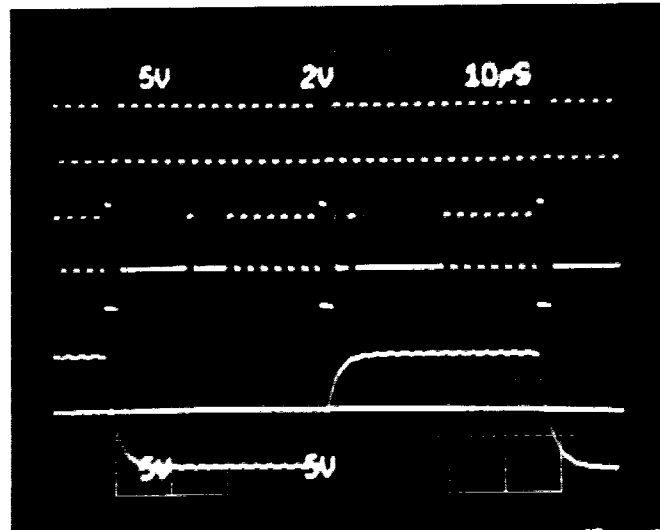
Fig. 21: Operation of the bipolar probe. The top trace is the 16-cycle input clock and the middle trace shows the input addresses and current level data. In this case, site #5 is selected and full-scale current is provided both sourcing and sinking (1111111). The bottom trace shows the measured voltage output waveform at site #5 across a 10kΩ resistor.
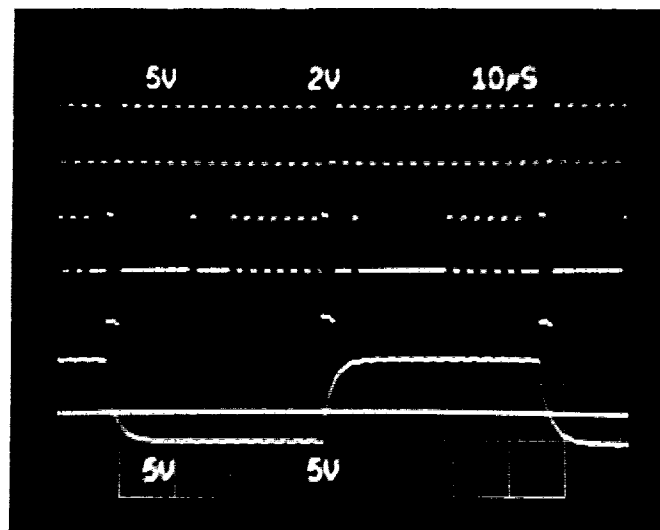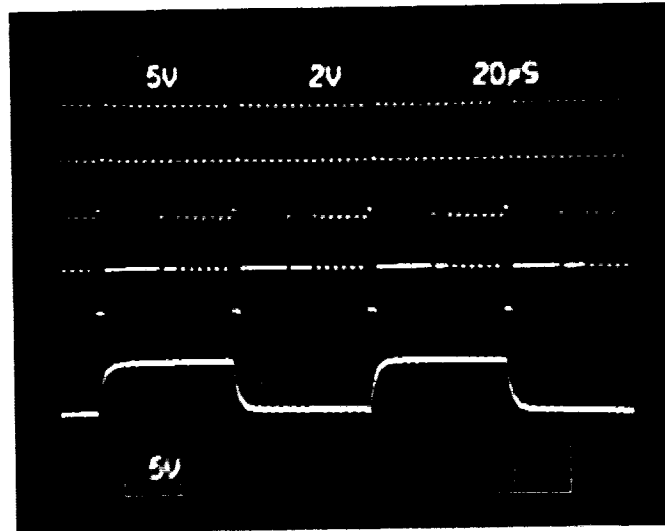

Fig. 22: Operation of the bipolar probe. The top trace is a 16-cycle input clock and the middle trace shows the input addresses and current level data. In this case, the current level is changed from (1111111) for sourcing to (0111111) for sinking. The bottom trace shows the measured voltage output waveform at site #5 across a 10kΩ resistor.

19

Fig. 23: Operation of the bipolar probe. The top trace is a 16-cycle input clock and the middle trace shows the input addresses and current level data. In this case, site #5 is selected and full-scale sourcing current (1111111) is provided while alternating different addresses: (100) to (010). The bottom trace shows the measured voltage output waveform at site #5 across a 10kΩ resistor.

PROCESS RESULTS

DC Device Characteristics

At this time, we focused our characterization on dc device characteristics such as the threshold voltage change after post-metallization processing (LTO and PECVD nitride deposition, electrode site formation (Ti/Ir), and the field dielectric etch processes) and the standby current characteristics. The latter have been a problem in the past. Table 2 summarizes the device characteristics after these thermal cycles. As can be seen in the table, the threshold voltage of each device decreases slightly (about -0.2V) and hence the current drive capability for each device increases (the maximum transconductance (gm_{max}) increases 1.5 to 4 times). This change might be due to the reduction of contact resistance after the thermal cycles. In the future we should anticipate this effect before the post-metal thermal cycles for the active probes. Figure 24 shows the current-voltage characteristics for (W/L)=(30μm/3μm) CMOS devices. Also, the use of a wide p-well separation and a thick n-epi layer has helped significantly reduce the standby current flow (from a few tens mA in STIM-1). Figure 25 shows the power supply current characteristics with various power supply voltages (Vcc in STIM-2). A power supply current of about 52μA was measured at Vcc=5V. This result makes low power electronics possible.

Table 2. Devices Characteristics before/after Thermal Cycle

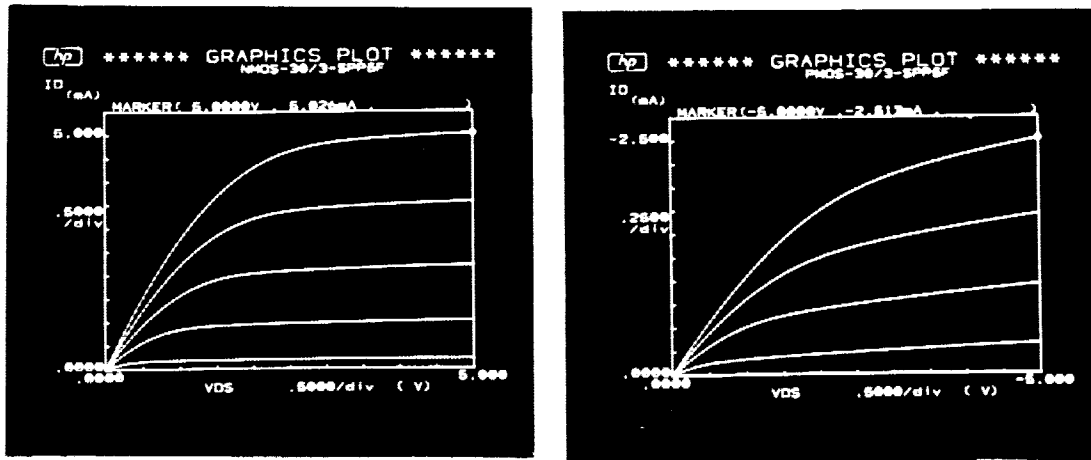| Devices	Before V_{TO}	After V_{TO}
NMOS	0.836V	0.628V
PMOS	-1.27V	-1.03V

Fig. 24: Current-voltage characteristics for W/L=30μm/3μm CMOS devices after final thermal cycles. (Right: pMOS; left: nMOS).
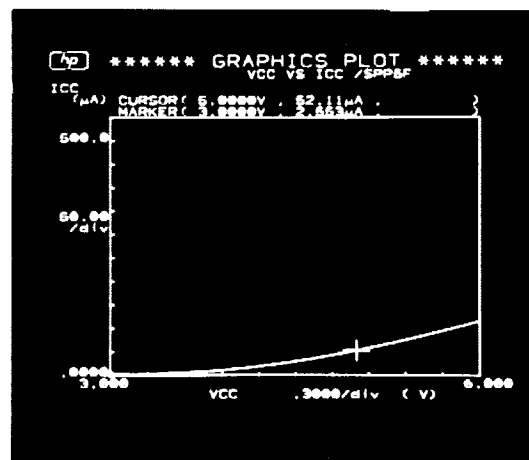

Fig. 25: Power supply current (Icc) in μA as a function of V_{cc}.

21

EDP Test Results

    In this run, we have coated working STIM probes with thick LTO (~1µm) and PECVD nitride (~0.5µm) and have etched the probes in EDP for 3.5hrs in order to check the top passivation layers. Figure 26 shows an SEM view of the surface topography of one of the LTO/PECVD-coated CMOS circuits after EDP, while Fig. 27 shows a cross-section of one of these probes after deposition of the upper dielectric layers (LTO/PECVD nitride). In this photo, the cross-section of a final shank is shown with LPCVD/LTO/PECVD dielectrics over the polysilicon interconnect line. The PECVD and the LTO and the LPCVD are distinguishable and together form a dielectric layer about 2.2µm thick. The step coverage appears to be excellent and no attack can be found even though the PECVD layer appears rather porous after the long EDP etch. Figure 28 shows one of the probe tips on STIM-2. The very sharp edges on these shanks are characteristic of the profiles produced by the shallow boron diffusion combined with a deep boron-diffused etch-stop.
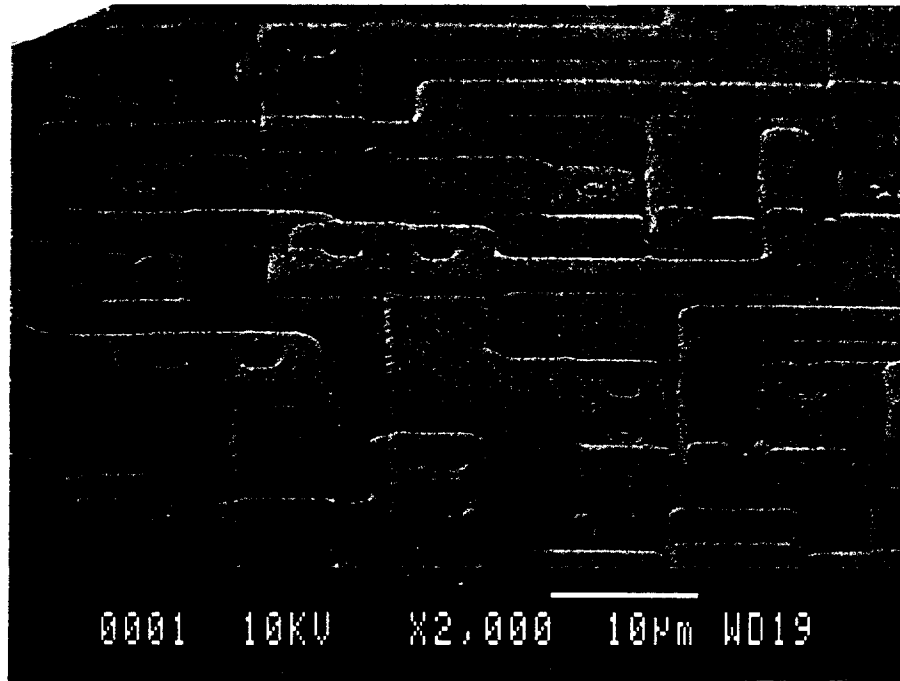

Fig. 26: SEM view of the surface topography of one of the LTO/PECVD-coated CMOS circuitry after EDP.
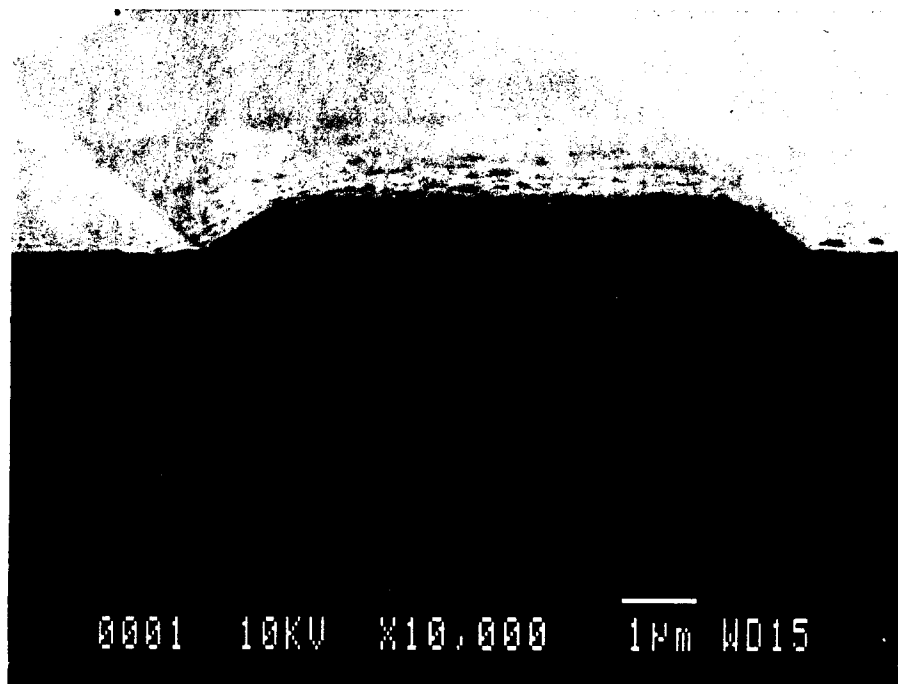
22

Fig. 27: Cross-section of one of these probes after deposition of the upper dielectric layers (LTO/PECVD nitride) on polysilicon interconnects.
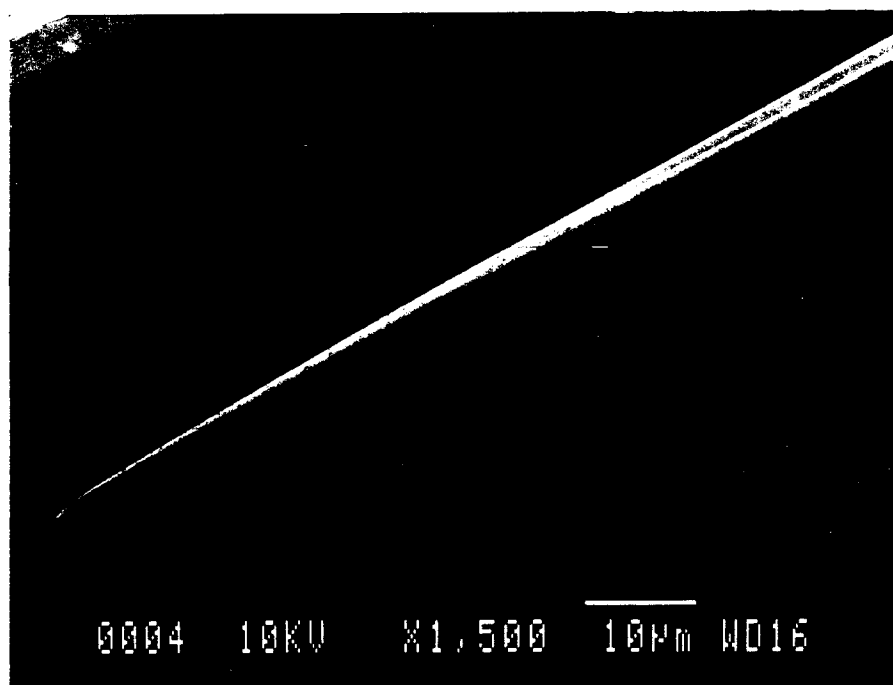

Fig. 28: One of the probe tips on STIM-2.

23

4. Conclusions

During the past quarter, additional "EMORY" and "HMRI" wafers have been completed successfully and have been characterized. The sites have exhibited normal impedance properties without the interfacial barriers observed on some previous wafers. These wafers include both recording and stimulating designs and have gold pads with either gold or iridium sites. Experiments on penetrating the pia arachnoid and dura mater with probes having a variety of tip shapes have begun with experiments in one guinea pig. Both shallow-boron-diffused and deep-boron-diffused probes penetrate the pia arachnoid quite readily, and the forces associated with the former are too low to be measured with our current strain gauges. No deformation of the cortical surface is seen. Neither of these probes penetrated dura, however, at least on the animal preparation used thus far. Additional experiments will be conducted during the coming quarter to obtain additional quantitative data on penetration as a function of probe shape.

Chronic experiments have continued during the past term to evaluate the access voltage associated with bipolar stimulation as a function of site size. The access voltages generally show only slight increases over five days of stimulation (4 hrs per day) and are about 8.5V for a $50\mu A$ pulse at $100\mu sec$/phase for a $1200\mu m^2$ site and about 8V for a $1600\mu m^2$ site. Histology results from the occipital lobe of one adult guinea pig stimulated at $50\mu A$ show significant tissue reaction, with a decreased number of neurons between tracts along with many reactive cells. This reaction was confined to the stimulated regions of tissue, with no cell loss or reactive cells and minimal glial reaction around the tracts remote from the active sites. Additional chronic studies are underway to confirm and expand on these findings.

Additional active probes have been fabricated using $1\mu m$-thick LTO films covered by $0.5\mu m$ of PECVD silicon nitride over the circuit areas. All probes are fully functional with no significant incidence of pinholes during final silicon etches of as long as 3.5hrs. Small threshold shifts of approximately -0.2V have been noted during the post-metal processing, possibly due to annealing of the contacts during the dielectric depositions. The first acute experiments with these active probes will take place during the coming term. A new fabrication run of active probes has also been started to correct the etching problems noted in earlier reports. These probes should be completed by the end of the coming quarter.